

atodes. However, further interpretation of these phylogenetic analyses is complicated by two considerations. First, clear MSP orthologs have not been identified outside of nematodes. Second, some proteins involved in sexual reproduction have been observed to undergo rapid evolution (21), which could eclipse evolutionary relationships. Thus, the current data do not allow us to distinguish between two alternative models. One possibility is that MSP arose from VAP during the evolution of the nematode reproductive system and diverged, acquiring one or multiple new functions. Alternatively, MSP was present in the common ancestor of many animals and was lost in some lineages or remains to be identified. MSP signaling functions could be derived and unique to MSP, or ancestral and shared among MSP and some VAP homologs. In any event, the exceptionally high degree of conservation in nematodes makes MSP an attractive anti-helminthic drug target.

Nematode sperm use a pseudopod to move over short distances by crawling (22). MSP is the most abundant protein in sperm (23) and forms self-assembling filaments in the pseudopod (24). Unlike flagellar sperm found in many animals, nematode sperm contain essentially no actin (25) and crawling is thought to be dependent on MSP function (26). The mechanism by which MSP signals are delivered to oocytes and sheath cells is not currently understood and may be novel. MSP does not have a signal sequence nor do *C. elegans* sperm have ribosomes, an endoplasmic reticulum, or a Golgi system (22). Pseudopod formation is not required for MSP signaling because *spe-4* spermatocytes (27), which fail to form pseudopods, are still capable of promoting oocyte maturation and sheath contraction (1).

These results, taken together with previous studies (24), indicate that MSP has acquired both extracellular signaling and intracellular cytoskeletal functions during evolution. MSP appears to perform these functions by mediating multiple protein-protein interactions using its single immunoglobulin-like fold (16, 28). The presence of MSP-like domains in yeast, plants, and animals suggests that some of these functions have been conserved during the evolution of multicellular organisms.

References and Notes

1. J. McCarter, B. Bartlett, T. Dang, T. Schedl, *Dev. Biol.* **205**, 111 (1999).
2. To prepare SCM, purified sperm (23) were incubated in M9 buffer (~5 × 10⁷ sperm per milliliter) for 1 to 16 hours at 20°C. Sperm were removed by centrifugation and filtration through a 0.22-μm cellulose acetate filter. After microinjection (~50 pl), oocyte maturation and sheath cell contraction rates were monitored by time-lapse video microscopy (1) for 70 min.
3. T. Schedl, J. Kimble, *Genetics* **119**, 43 (1988).
4. Web movies 1 through 4 and Web fig. 1 are available

at *Science* Online at www.sciencemag.org/cgi/content/full/291/5511/2144/DC1.

5. SCM or sperm lysates, prepared by vortexing with glass beads, were fractionated on C₄ and C₁₈ columns (Vydac, Hesperia, CA) using an acetonitrile gradient (0 to 100%) mobile phase containing 0.1% trifluoroacetic acid. Absorbance peaks (214 nm) were collected manually, dialyzed against M9, and bioassayed.
6. Active fractions were analyzed by MALDI-TOF mass spectrometry. Post source decay mass spectrometry (29) of a 1960-dalton peptide, generated by tryptic digestion of the active fraction, yielded the sequence IVFNAPYDDKHTYHIK (30), matching MSP.
7. S. Ward *et al.*, *J. Mol. Biol.* **199**, 1 (1988).
8. M. Miller, V. Nguyen, R. Caprioli, D. Greenstein, unpublished data.
9. His-tagged MSP-77, MSP-38, and MSP(1 to 106) were purified under native conditions by Ni-nitrilotriacetic acid (Ni-NTA) (Qiagen, Valencia, CA) affinity chromatography (>99% pure by SDS-PAGE and MALDI-TOF). MSP concentrations were determined by amino acid hydrolysis, SDS-PAGE, and spectrophotometrically using ϵ (275 nm) = 3.29 × 10⁴ M⁻¹ cm⁻¹.
10. Antibodies to MSP (23) or EMB-30 control antibodies were injected (~40 μg/ml) into wild-type adult hermaphrodites (24 hours post-L4 at 20°C), which were then cultured individually with food for 3 hours. Total ovulations were determined (7) and oocyte maturation was analyzed by time-lapse video microscopy. A two-sample *t* test was used to assess statistical significance.
11. K. L. Hill, S. W. L'Hernault, *Dev. Biol.* **232**, 105 (2001).
12. The COOH-terminal MSP peptide (REWFQGDGMVR-RKNLPIEYNP) (30) was prepared by solid-phase synthesis and purified by HPLC.
13. J. E. Ferrell Jr., *Bioessays* **21**, 833 (1999).
14. Diphosphorylated MPK-1 was detected using indirect immunofluorescence with the antibody MAPK-YT (37) (Sigma). Dissected and fixed (3% paraformaldehyde) gonads were stained 40 min post MSP injection.
15. M. R. Lackner, S. K. Kim, *Genetics* **150**, 103 (1998).
16. T. L. Bullock, T. M. Roberts, M. Stewart, *J. Mol. Biol.* **263**, 284 (1996).

17. P. A. Skehel, K. C. Martin, E. R. Kandel, D. Bartsch, *Science* **269**, 1580 (1995).
18. L. Soussan *et al.*, *J. Cell Biol.* **146**, 301 (1999).
19. J. Ramalho-Santos *et al.*, *Dev. Biol.* **223**, 54 (2000).
20. J. R. Schultz, J. D. Sasaki, V. D. Vacquier, *J. Biol. Chem.* **273**, 24355 (1998).
21. V. D. Vacquier, *Science* **281**, 1995 (1998).
22. S. W. L'Hernault, in *C. elegans II*, D. L. Riddle, T. Blumenthal, B. J. Meyer, J. R. Priess, R., Eds. (Cold Spring Harbor Laboratory Press, Cold Spring Harbor, NY, 1997), pp. 271–294.
23. M. R. Klass, D. Hirsh, *Dev. Biol.* **84**, 299 (1981).
24. T. M. Roberts, M. Stewart, *J. Cell Biol.* **149**, 7 (2000).
25. G. A. Nelson, T. M. Roberts, S. Ward, *J. Cell Biol.* **92**, 121 (1982).
26. J. E. Italiano Jr., T. M. Roberts, M. Stewart, C. A. Fontana, *Cell* **84**, 105 (1996).
27. S. W. L'Hernault, P. M. Arduengo, *J. Cell Biol.* **119**, 55 (1992).
28. H. E. Smith, S. Ward, *J. Mol. Biol.* **279**, 605 (1998).
29. R. Kaufmann, B. Spengler, F. Lutzenkirchen, *Rapid Comm. Mass Spectrom.* **7**, 902 (1993).
30. Single-letter abbreviations for the amino acid residues are as follows: A, Ala; C, Cys; D, Asp; E, Glu; F, Phe; G, Gly; H, His; I, Ile; K, Lys; L, Leu; M, Met; N, Asn; P, Pro; Q, Gln; R, Arg; S, Ser; T, Thr; V, Val; W, Trp; and Y, Tyr.
31. Y. Yung *et al.*, *FEBS Lett.* **408**, 292 (1997).
32. We thank S. Ward for providing antibodies and Y. Kohara for expressed sequence tag clones. Some strains used in this study were provided by the *Caenorhabditis* Genetics Center, which is supported by NIH. We thank D. Bridge, C. Desai, B. Hogan, D. Miller, and R. Steele for helpful discussions and review of the manuscript. We thank E. Mitchell for digital video editing. M.A.M. and M.K. were supported by NIH training grants HD07043 and CA09592. Supported by grants from NIH (GM57173 to D.G., GM58008 to R.M.C., and HD25614 to T.S.).

20 November 2000; accepted 7 February 2001

Sonic Hedgehog Control of Size and Shape in Midbrain Pattern Formation

Seema Agarwala, Timothy A. Sanders, Clifton W. Ragsdale*

Little is known about how patterns of cell types are organized to form brain structures of appropriate size and shape. To study this process, we employed *in vivo* electroporation during midbrain development to create ectopic sources of Sonic Hedgehog, a signaling molecule previously shown to specify different neuronal cell types in a concentration-dependent manner *in vitro*. We provide direct evidence that a Sonic Hedgehog source can control pattern at a distance in brain development and demonstrate that the size, shape, and orientation of the cell populations produced depend on the geometry of the morphogen source. Thus, a single regulatory molecule can coordinate tissue size and shape with cell-type identity in brain development.

The determination of cell fate and the spatial organization of differentiated cells are the fundamental processes by which any tissue is organized during development. An attractive

mechanism for achieving spatial patterns of different neuronal cell types is through a “positional signal” from a morphogen source that elicits distinct molecular responses in target cells according to their distance from that source (1, 2). Evidence that Sonic Hedgehog (SHH) can serve as a positional signal in vertebrate central nervous system (CNS) development has come mainly from *in vitro* studies demonstrating that different cell

Department of Neurobiology, Pharmacology, and Physiology, The University of Chicago, Chicago, IL 60637, USA.

*To whom correspondence should be addressed. E-mail: cliff@drugs.bsd.uchicago.edu

types in spinal cord explant cultures can be produced by different concentrations of recombinant SHH (3–5). We have sought in vivo evidence for positional signaling by SHH in brain development.

To demonstrate SHH effects on brain development, we employed controlled electro-

porations to express *SHH* ectopically in chick midbrain at embryonic day 2 (E2), an age when endogenous *SHH* gene expression is restricted to the ventral midline (Fig. 1A). The embryonic ventral midbrain is an attractive system for studying brain patterning, because it is transiently organized into a regular

set of discrete arcuate territories (midbrain arcs) arrayed bilateral to the ventral midline (6). Each of these arcuate territories has a unique molecular identity, based on its expression of specific transcription factors. We assessed the effects of our electroporations at E5, when five molecularly distinct territories can be identified (Fig. 1, B through E). From the ventral midline outward, these territories are arc 1 (marked by *PHOX2A*⁺ motoneurons), arc 2 (*GATA2*⁺, *FOXA2*⁺), the *PAX6* stripe, arc 3 (*GATA2*⁺, *FOXA2*⁺), and the *EVX1* stripe. By employing multiple probe wholemount in situ hybridization, we examined the effects of *SHH* misexpression on midbrain patterning as a whole, rather than on single cell types. Electroporations with alkaline phosphatase cDNA showed that we could make half of the ventral midbrain transgenic, with the other half serving as a control (Fig. 2A). In addition, electroporation itself did not disrupt midbrain arc patterning (Fig. 2B).

We first studied the effects of enlarging the *SHH* territory in ventromedial midbrain (7). As expected (8–10), *SHH* overexpression led to the up-regulation of transcriptional targets of SHH, including *FOXA2/HNF3β* and the SHH receptor *PATCHED* (Fig. 2, C and D). In addition, the entire arcuate pattern of the ventral midbrain, including the *PHOX2A*⁺ motoneurons of arc 1 and the *GATA2*⁺ lateral arcs, was expanded (Fig. 2, E and F). Despite these expansions, the relative positions of the arcuate territories to each other and to the *SHH* source were maintained.

SHH misexpression stimulated cell proliferation (Fig. 2G) and produced frank tissue growth of the ventral midbrain (Fig. 2H).

Fig. 1. *SHH* gene expression and midbrain arc anatomy. (A and B) Nested expression of *SHH* (blue) and *FOXA2/HNF3β* (brown) in E2 brain (A) and E5 midbrain (B). *SHH* and *FOXA2* gene expression were used interchangeably to determine extent of *SHH* misexpression. In all photomicrographs, dissected brains are presented as flattened wholemounts, with rostral to the top and the ventricular surface facing the viewer. The genes detected with two-color in situ hybridization (20) are noted by color-coded text at the bottom right of each panel. (C to E) Five molecularly distinguished arcuate territories are identified in the E5 ventral midbrain mantle layer (see text). (C) The *PHOX2A*⁺ arc 1 is spatially segregated from the *GATA2*⁺ lateral arcs 2 and 3. (D) Spatial relationship of *SHH*, arcs 1 through 3, and homeobox (*Hx*) gene expression of *PHOX2A* (P2), *PAX6* (P6), and *EVX1* (E1). (E) Cartoon summary of gene expression patterns for *SHH* (brown), *FOXA2* (dark gray) and arc-specific transcription factors at E5. Domains of *SHH* and *FOXA2* gene expression are exaggerated caudally to illustrate the spatial relationships of the markers. The rostral extensions of the *SHH* and *FOXA2* into diencephalon are omitted. III, third ventricle; FB, forebrain; FP, hindbrain floor plate; HB, hindbrain; IS, isthmus; rFP, rostral (or midbrain) floor plate.

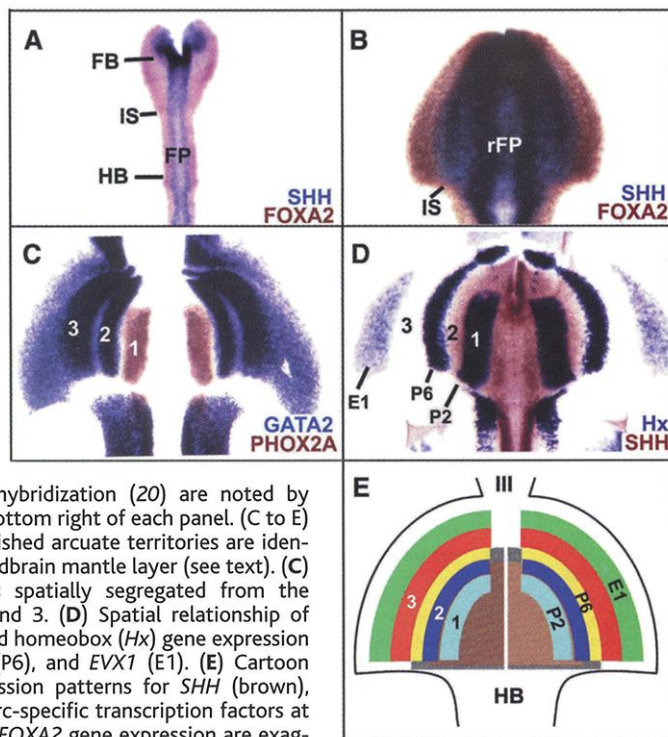


Fig. 2. *SHH* misexpression in ventral midbrain. (A and B) Outcome of unilateral control electroporations at E2.5. (A) Alkaline phosphatase (AP) transgene expression at E5 shows AP transfection encompassing one entire side of the ventral midbrain. Electroporated side in this and subsequent panels is the right. (B) E5 arc pattern identified by *Hx* gene expression is not disrupted by electroporation. *PAX3* gene expression marks midbrain tectum, which surrounds the midbrain arcs in flattened whole-mounts. [(C) to (H)] Effects of *SHH* electroporation at E2. (C and D) Expanded gene expression of *SHH* and *FOXA2* (C), and *PATCHED* (*PTC*) (D) at E5. (E and F) Expanded *PHOX2A* and *GATA2* gene expression at E5. Little overlap is seen between the *PHOX2A*⁺ motoneurons in arc 1 and the *GATA2*⁺ lateral arcs regardless of the nature of the enlargement of the *SHH* source. Note that the arc expansions include increases of both length (F) and width (E and F). (G) Increased BrdU labeling (21) over the *PHOX2A*⁺ territory at E3. (H) Enlarged right midbrain at E9. The outline of the control left ventral midbrain is imposed (black dots) on the electroporated side to illustrate the increase in midbrain tissue mass. Expanded *ISL1*⁺ motoneuron population (right) confirms successful *SHH* electroporation. TEC, tectum.

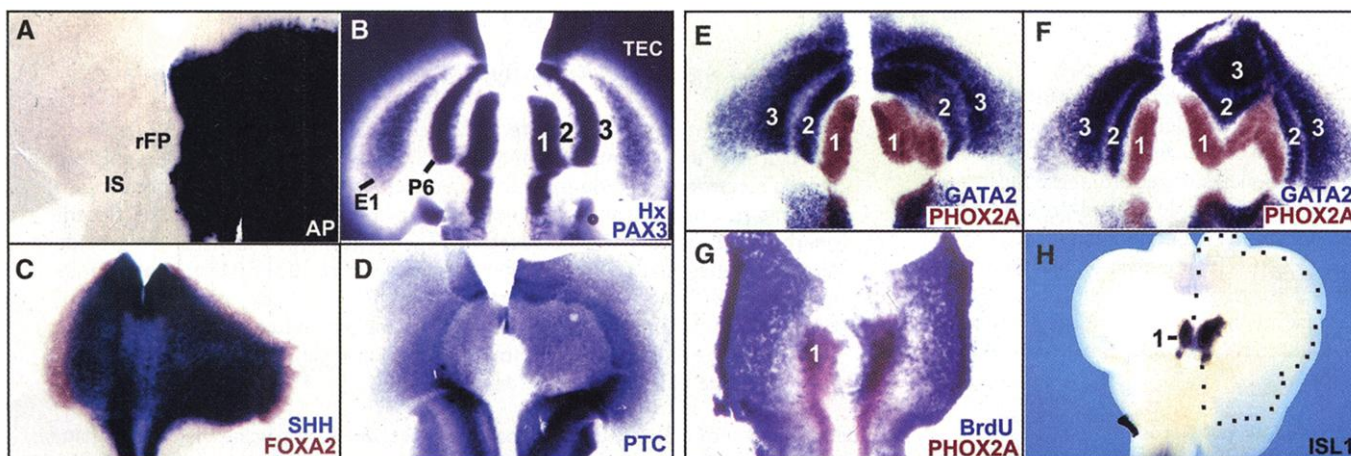


Fig. 2. *SHH* misexpression in ventral midbrain. (A and B) Outcome of unilateral control electroporations at E2.5. (A) Alkaline phosphatase (AP) transgene expression at E5 shows AP transfection encompassing one entire side of the ventral midbrain. Electroporated side in this and subsequent panels is the right. (B) E5 arc pattern identified by *Hx* gene expression is not disrupted by electroporation. *PAX3* gene expression marks midbrain tectum, which surrounds the midbrain arcs in flattened whole-mounts. [(C) to (H)] Effects of *SHH* electroporation at E2. (C and D) Expanded gene expression of *SHH* and *FOXA2* (C), and *PATCHED* (*PTC*) (D) at E5. (E and F) Expanded

PHOX2A and *GATA2* gene expression at E5. Little overlap is seen between the *PHOX2A*⁺ motoneurons in arc 1 and the *GATA2*⁺ lateral arcs regardless of the nature of the enlargement of the *SHH* source. Note that the arc expansions include increases of both length (F) and width (E and F). (G) Increased BrdU labeling (21) over the *PHOX2A*⁺ territory at E3. (H) Enlarged right midbrain at E9. The outline of the control left ventral midbrain is imposed (black dots) on the electroporated side to illustrate the increase in midbrain tissue mass. Expanded *ISL1*⁺ motoneuron population (right) confirms successful *SHH* electroporation. TEC, tectum.

Thus, the observed patterning effects could be due to the expansion of pools of dedicated precursor cells rather than the respecification of cell fates by SHH. Consequently, we used microelectroporation to create small sources of ectopic SHH in dorsal midbrain, where arcs are never seen. These experiments established that an ectopic SHH source is sufficient to elicit a complete set of midbrain arcs (Fig. 3, A and B).

To explore the mechanism by which SHH generates multiple midbrain cell types, we introduced sources of SHH within the ventral midbrain at varying distances from the ventral midline. When placed in lateral tectum, the ectopic SHH source produced a complete mirror-image duplication of the arc pattern (Fig. 3C). As the two SHH sources were brought close together, however, cell types normally occupying arcuate territories most distant from the SHH source, such as arc 3 and the EVX1 territory, were lost from the center of the pattern (Fig. 3D), suggesting that the level of the signal provided by the two nearby SHH sources is too high to specify arc 3 or the EVX1 territory. Thus, a SHH source does not simply induce the midbrain arc pattern, but provides a positional signal to specify cell-type identity.

The next set of experiments explored how

a positional signal controlling cell-type specification could be deployed to produce brain structures of the required shape and orientation. In hindbrain and spinal cord development, most neuronal cell types are arranged into longitudinal columns bilateral to the ventral midline. A simple account of this patterning is that the SHH in the ventral midline provides a positional signal and that the read-outs of this signal are longitudinal columns because the source is a longitudinal stripe. Shifting the orientation of the SHH source by 90° should still produce a parallel array of stripes, but they should lie perpendicular to the normal arc pattern. By microelectroporation, we directed ectopic SHH to the isthmus (midbrain-hindbrain junction), creating a morphogen source orthogonal to the ventral midline. The ectopic arcs ran perpendicular to the normal arcs, forming an L-shaped pattern of midbrain cell types that conformed to the L-shaped SHH source (Fig. 3E). Thus, the orientation of the SHH source determines the orientation of the arc pattern.

If a line source of SHH elicits stripes, then a spot source should produce a radial pattern. Such patterns have been demonstrated with morphogens of the TGFβ family (11, 12). We found that microelectroporations producing spots of SHH gene expression created bull's-

eye patterns of arc-specific rings, which resembled the eyespot of a butterfly's wing (Fig. 3F). Eyespots are known to express hedgehog transcripts (13) and to function as organizers in transplant experiments (14). Our findings establish that ectopic hedgehog is sufficient to organize an eyespot-like pattern in epithelial tissue.

Finally, we found that small SHH sources elicited small patterns of ectopic arcs and large sources produced large patterns (Fig. 4). In essence, the size of the SHH source sets up the size of the field of ectopic arcs and the sizes of the individual arcuate territories.

Our findings provide evidence that a SHH positional signal is able to establish a complete pattern of ventral midbrain cell types. We also demonstrate that SHH in brain development, like *hh*, *wg*, and *dpp* in *Drosophila* limb development (15–17), can coordinate patterning with size control. Our results further point to the critical role that the geometry of a morphogen source plays in patterning vertebrate CNS structures and suggest a reason why the development of the floor plate, the principal source of SHH in spinal cord and brainstem development, is under such extensive developmental regulation (18, 19). To pattern the CNS correctly, not only the location, but also the shape and size, of the SHH source must be precise because the consequences for the patterning of neuronal assemblies are profound. In spinal cord development, SHH is expressed in a tight mid-

Fig. 3. SHH serves as a positional signal in midbrain pattern formation. (A and B) An ectopic SHH source is sufficient to elicit a full set of tegmental arcs. (A) Side view of an E5 brain showing ectopic arcs (arrowhead) in lateral tectum. Arrow indicates position of normal arcs in ventral midbrain. Rostral is to the right. (B) Dorsal view of an E5 brain showing a complete ectopic arc pattern in caudal tectum. Rostral is to the top. Isthmus (blue) identified by *WNT1* gene expression. (C and D) Respecification of ventral midbrain cell types as an ectopic source of SHH is moved toward the endogenous SHH source. (C) Ectopic SHH in lateral tectum, assayed by *FOXA2* gene expression, results in a mirror-image duplication of the normal arc pattern. (D) As the distance between the two sources is reduced, only a partial duplication of the arc pattern results. Arc 3 and the *EVX1* territory are present on both sides of the merged pattern, but are lost from the center of this "contour map" of SHH positional signaling. (E) Orientation of the SHH source determines the orientation of the pattern. An ectopic SHH source concentrated along the isthmus elicits arcs arrayed parallel to the isthmus and at 90° to the axis of the normal arc pattern. (F) The shape of the SHH source determines the shape of the pattern. A spot source of SHH produces a bull's-eye pattern of gene expression. Tr, trochlear nucleus.

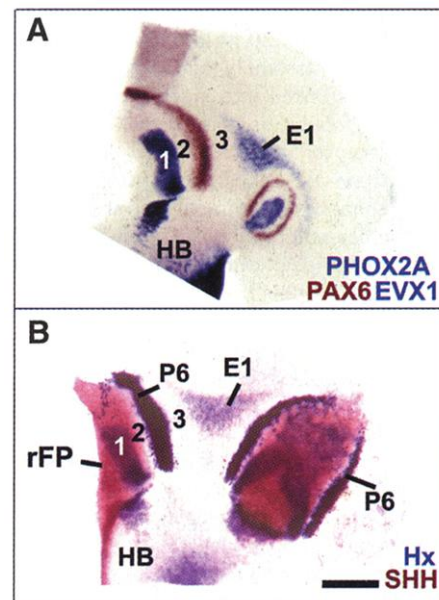
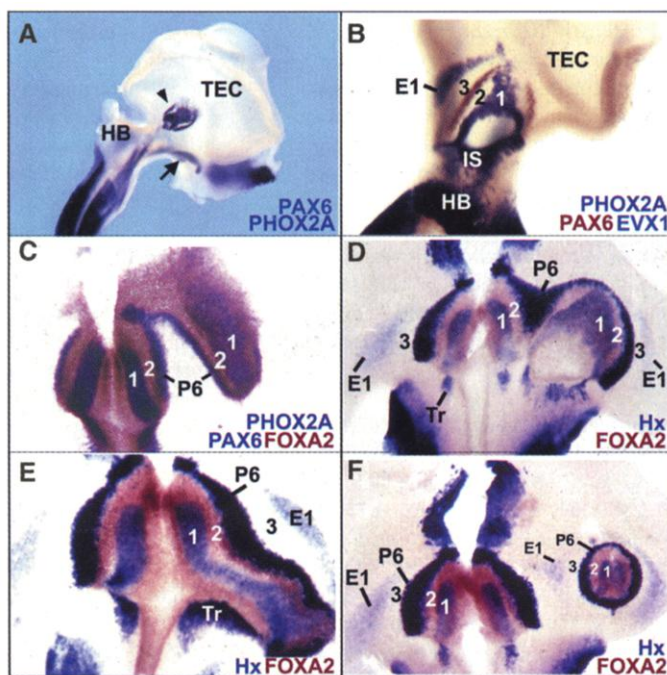


Fig. 4. The size of the ectopic arc pattern is determined by the size of the SHH source. (A and B) *Hx* gene expression shows that small (A) or large (B) arc patterns can be produced and that the size of the pattern is proportional to the size of the SHH source (B). The right ventral midbrain and the part of tectum containing the ectopic pattern are shown in each flat-mount. Ventral midline is to the left. Bar, 448 μm.

line stripe and longitudinal columns are formed. By contrast, in midbrain development, *SHH* expression fans out from the ventral midline, and arcuate territories in register with the morphogen source are the result.

References and Notes

1. L. Wolpert, *J. Theor. Biol.* **25**, 1 (1969).
2. L. Wolpert, *Trends Genet.* **12**, 359 (1996).
3. J. Briscoe, J. Ericson, *Semin. Cell. Dev. Biol.* **10**, 353 (1999).
4. H. Roelink *et al.*, *Cell* **76**, 761 (1994).
5. E. Marti, D. A. Bumcrot, R. Takada, A. P. McMahon, *Nature* **375**, 322 (1995).
6. T. Sanders, A. Lumsden, C. Ragsdale, in preparation.
7. The *SHH* expression plasmid contained a cDNA encoding the 19.2-kD NH₂-terminal fragment of chick SHH [R. D. Riddle, R. L. Johnson, E. Laufer, C. Tabin, *Cell* **75**, 1401 (1993)] inserted into the expression vector pXcX [A. D. Johnson, P. A. Krieg, *Dev. Genet.* **17**, 280 (1995)]. Our results are based on whole-mount in situ hybridization analysis of 794 embryos transgenic for *SHH* expression. In 101 of the brains, *SHH* or its transcriptional target *FOXA2* (8) was de-

8. Y. Echelard *et al.*, *Cell* **75**, 1417 (1993).
9. V. Marigo, M. P. Scott, R. L. Johnson, L. V. Goodrich, C. J. Tabin, *Development* **122**, 1225 (1996).
10. Y. Watanabe, H. Nakamura, *Development* **127**, 1131 (2000).
11. T. Lecuit, S. M. Cohen, *Development* **125**, 4901 (1998).
12. J. B. Gurdon, P. Harger, A. Mitchell, P. Lemaire, *Nature* **371**, 487 (1994).
13. D. N. Keys *et al.*, *Science* **283**, 532 (1999).

14. H. F. Nijhout, *Dev. Biol.* **80**, 267 (1980).
15. K. Basler, G. Struhl, *Nature* **368**, 208 (1994).
16. B. A. Edgar, C. F. Lehner, *Science* **274**, 1646 (1996).
17. S. J. Day, P. A. Lawrence, *Development* **127**, 2977 (2000).
18. M. Placzek, J. Dodd, T. M. Jessell, *Curr. Opin. Neurobiol.* **10**, 15 (2000).
19. N. M. Le Douarin, M. E. Halpern, *Curr. Opin. Neurobiol.* **10**, 23 (2000).
20. E. A. Grove, S. Tole, J. Limon, L. Yip, C. W. Ragsdale, *Development* **125**, 2315 (1998).
21. Embryos were collected 30 min after an intravenous bromodeoxyuridine (BrdU) pulse and processed for in situ hybridization and antibody detection of BrdU-labeled cells.
22. We thank A. M. Greenlee for technical assistance, E. Ferguson, E. Grove, P. Mason, and V. Prince for discussions and C. Cepko, D. Engel, C. Goridis, M. Goulding, T. Jessell, A. Johnson, G. Martin, A. McMahon, and C. Tabin for cDNAs. Supported by National Institute of Neurological Disorders and Stroke (NIH).

26 December 2000; accepted 7 February 2001
 Published online 1 March 2001;
 10.1126/science.1058624
 Include this information when citing this paper.

Structure of an Extracellular gp130 Cytokine Receptor Signaling Complex

Dar-chone Chow,¹ Xiao-lin He,¹ Andrew L. Snow,¹ Stefan Rose-John,² K. Christopher Garcia^{1*}

The activation of gp130, a shared signal-transducing receptor for a family of cytokines, is initiated by recognition of ligand followed by oligomerization into a higher order signaling complex. Kaposi's sarcoma-associated herpesvirus encodes a functional homolog of human interleukin-6 (IL-6) that activates human gp130. In the 2.4 angstrom crystal structure of the extracellular signaling assembly between viral IL-6 and human gp130, two complexes are cross-linked into a tetramer through direct interactions between the immunoglobulin domain of gp130 and site III of viral IL-6, which is necessary for receptor activation. Unlike human IL-6 (which uses many hydrophilic residues), the viral cytokine largely uses hydrophobic amino acids to contact gp130, which enhances the complementarity of the viral IL-6-gp130 binding interfaces. The cross-reactivity of gp130 is apparently due to a chemical plasticity evident in the amphipathic gp130 cytokine-binding sites.

In vertebrates, gp130 is a shared signal-transducing receptor for a family of cytokines, including IL-6, herpesvirus IL-6 (vIL-6), IL-11, ciliary neurotrophic factor (CNTF), cardiotrophin (CT-1), leukemia inhibitory factor (LIF), oncostatin (OSM), and NNT-1/BSF3, which mediate a wide variety of both overlapping and unique biological responses in vivo (1-4). The activities of gp130 cytokines are mediated through formation of oligomeric complexes containing one or more copies of

gp130, which leads to intracellular activation of Src and Janus tyrosine kinases and of the STAT family of transcription factors (3, 5, 6).

Cytokines that activate gp130 share a common, four-helix bundle fold (7, 8). Engagement of gp130 occurs through three conserved receptor-binding epitopes on the cytokines, the third of which is unique to gp130 cytokines (9-13). By analogy to other hematopoietic cytokine receptors, gp130 is presumed to recognize ligand through its cytokine-binding homology region (CHR), located at domains 2 and 3 (D2D3) (8, 11-14). However, gp130 uniquely requires an additional NH₂-terminal (D1) immunoglobulin (Ig)-like activation domain (IGD) in order to be functionally responsive to cytokine (15).

Hematopoietic receptors such as human growth hormone (hGH) exhibit a simple ac-

tivation model characterized by the homodimerization of two receptors by one cytokine molecule via binding sites I and II (16, 17). In contrast, for gp130, "recognition" and "activation" complexes are disparate hetero-oligomeric species that are formed in a step-wise fashion (11-13, 18, 19). IL-6, the most extensively studied of the gp130 cytokines, cannot bind gp130 unless it first forms a complex with a specific α receptor (termed IL-6R α , hereafter simply R α) through a "site I" epitope (3). This binary IL-6-R α complex forms a composite epitope, termed "site II," which interacts with the CHR of gp130 (D2D3 domains) to form a trimolecular (1:1:1) recognition complex, which is not competent for signaling. A transition to a higher order signaling assembly requires recruitment of the site III epitope and IGD into the recognition complex to form the higher order activation complex (10, 15, 20, 21). Although the topology of the activated assembly remains unknown, functional studies indicate that IL-6 and IL-11 signaling complexes are "hexamers" containing two copies each of cytokine, R α , and gp130 (2:2:2) (18, 22, 23). Because the functional epitopes (sites I, II, and III) of all gp130 cytokines are in similar locations, it is likely that each signaling assembly will be constructed from a common oligomeric template.

Kaposi's sarcoma-associated herpesvirus (KSHV, or HHV8) is a recently discovered γ -herpesvirus that is a likely causative factor for the development of acquired immunodeficiency syndrome-related Kaposi's sarcoma (KS), as well as other neoplastic diseases associated with KS (24). KSHV encodes a functional homolog of interleukin-6 (termed vIL-6, 25% sequence homology) that is expressed in KS-infected cells and is able to induce angiogenesis and hematopoiesis in IL-6-dependent cell lines (25, 26). vIL-6 direct-

¹Department of Microbiology and Immunology and Department of Structural Biology, Stanford University School of Medicine, Fairchild D319, 299 Campus Drive, Stanford, CA 94305, USA. ²Department of Biochemistry, Christian-Albrechts-Universität zu Kiel, Olshausenstraße 40, D-24098 Kiel, Germany.

*To whom correspondence should be addressed. E-mail: kcgarcia@stanford.edu